EARTH SURFACE PROCESSES AND LANDFORMS
Earth Surf. Process. Landforms **41**, 1358–1369 (2016)

Published online 19 February 2016 in Wiley Online Library
(wileyonlinelibrary.com) DOI: 10.1002/esp.3906

Field application of close-range digital photogrammetry (CRDP) for grain-scale fluvial morphology studies

Stephane Bertin* and Heide Friedrich
Department of Civil and Environmental Engineering, The University of Auckland, Auckland, New Zealand

Received 4 August 2015; Revised 17 January 2016; Accepted 18 January 2016

*Correspondence to: Stephane Bertin, Department of Civil and Environmental Engineering, The University of Auckland, Auckland, New Zealand. E-mail: s.bertin@ymail.com

ESPL
Earth Surface Processes and Landforms

ABSTRACT: *In situ* measurement of grain-scale fluvial morphology is important for studies on grain roughness, sediment transport and the interactions between animals and the geomorphology, topics relevant to many river practitioners. Close-range digital photogrammetry (CRDP) and terrestrial laser scanning (TLS) are the two most common techniques to obtain high-resolution digital elevation models (DEMs) from fluvial surfaces. However, field application of topography remote sensing at the grain scale is presently hindered mainly by the tedious workflow challenges that one needs to overcome to obtain high-accuracy elevation data. A recommended approach for CRDP to collect high-resolution and high-accuracy DEMs has been developed for gravel-bed flume studies. The present paper investigates the deployment of the laboratory technique on three exposed gravel bars in a natural river environment. In contrast to other approaches, having the calibration carried out in the laboratory removes the need for independently surveyed ground-control targets, and makes for an efficient and effective data collection in the field. Optimization of the gravel-bed imagery helps DEM collection, without being impacted by variable lighting conditions. The benefit of a light-weight three-dimensional printed gravel-bed model for DEM quality assessment is shown, and confirms the reliability of grain roughness data measured with CRDP. Imagery and DEM analysis evidences sedimentological contrasts between gravel bars within the reach. The analysis of the surface elevations shows the effect variable grain-size and sediment sorting have on the surface roughness. By plotting the two-dimensional structure functions and surface slopes and aspects we identify different grain arrangements and surface structures. The calculation of the inclination index allows determining the surface-forming flow direction(s). We show that progress in topography remote sensing is important to extend our knowledge on fluvial morphology processes at the grain scale, and how a technique customized for use by fluvial geomorphologists in the field benefits this progress. Copyright © 2016 John Wiley & Sons, Ltd.

KEYWORDS: fieldwork; gravel-bed river; photogrammetry; DEM; grain roughness

Introduction

Studies on the geomorphology of gravel-bed rivers at the grain scale and the measurement of gravel patches have seen a growing interest over the last decades, due to progress in high-resolution remote sensing. Digital elevation models (DEMs), analysed using the standard deviation of bed elevations, can potentially replace tedious sediment sampling in the field and improve grain-roughness parameterization needed for hydraulic and sediment transport calculations (Nikora *et al.*, 1998; Aberle and Smart, 2003; Entwistle and Fuller, 2009; Heritage and Milan, 2009). Likewise, collection of high-resolution DEMs from distinct hydraulic biotopes (e.g. riffles and pools, or bars and pools, exposed at the time of measurement) was critical in characterizing the links between morphological units, sediment transport and surface structure (Hodge *et al.*, 2009a; Hodge *et al.*, 2013) and to quantify the 'patchy' nature of gravel surfaces (Nelson *et al.*, 2010). With only traditional field sampling of surface composition, crucial information on particle exposure, imbrication and surface roughness cannot be derived. Measuring microtopographic relief is also important as it provides means to assess aquatic habitats and the relation between species and the geomorphology (Du Preez and Tunnicliffe, 2012; Rice *et al.*, 2012; Hannam and Moskal, 2015).

Close-range digital photogrammetry (CRDP), i.e. the combination of using one or more digital cameras and subsequent image matching to obtain surface elevations at the image overlap, and 'time-of-flight' terrestrial laser-scanning (TLS), are presently the most commonly used remote-sensing techniques, able to measure gravel-bed topography with a sufficient amount of detail at the grain scale (spatial resolution approximate in millimetres). Both techniques have been used in both laboratory and field settings, and have been shown capable of measuring shallow riverbed microtopography (Butler *et al.*, 2002; Smith *et al.*, 2012; Bertin *et al.*, 2013; Smith and Vericat, 2014). However, the latter is seldom used, mainly due to degraded DEM quality compared to conventional in-air measurement. In addition, this application comes with substantial experimental difficulties. Generally, studied surfaces are exposed gravel bars at low flow or in drained laboratory flumes. When it comes to field applications, various methodological attributes may be considered to decide which technique

to adopt. The most important aspect is the need to obtain fit-for-purpose topography data, which are suitable for the intended analysis. In other words, what is a sufficient measurement accuracy and precision to improve our knowledge of fluvial microtopography? For measuring fluvial surfaces at the grain scale, both CRDP and TLS methodologies require the greatest care to mitigate errors in elevation data (Hodge *et al.*, 2009b; Bertin *et al.*, 2015), errors which otherwise may affect findings (Lane *et al.*, 2005; James *et al.*, 2007). Repeating scans, in addition to applying erroneous points filtering techniques (Hodge *et al.*, 2009b), is currently the best option to reduce errors and improve accuracy for TLS applications, with the measuring precision otherwise being dependent on the used instrument and software. The challenge with CRDP is the development of a stable workflow from image acquisition to surface structure data (Lane, 2000; Lane *et al.*, 2000; Chandler *et al.*, 2005; Wackrow *et al.*, 2007). Presently, a variety of DEM reconstruction techniques are available, from the now conventional digital stereo (i.e. two-camera) photogrammetry, using either commercial (Lane, 2000; Lane *et al.*, 2000; Butler *et al.*, 2002; Chandler *et al.*, 2005; Bird *et al.*, 2010) or non-proprietary (Bertin *et al.*, 2013; Bouratsis *et al.*, 2013; Bertin *et al.*, 2014, 2015) calibration and stereo-matching engines, to novel structure-from-motion (SfM) or multi-view stereo (MVS) photogrammetry (James and Robson, 2012; Fonstad *et al.*, 2013; Javernick *et al.*, 2014), which does not need calibration but has not been tested on a gravel patch yet. Recent progress was made in the laboratory, showing that the use of non-proprietary digital stereo photogrammetry optimizes the workflow, which when done appropriately, can result in sub-millimetre accurate gravel-bed DEMs (Bertin *et al.*, 2015) – a development that is yet to be tested in a natural river environment. Compared to applying CRDP in the laboratory, the ease with which data are collected in the field is also becoming more important, in addition to the quality of obtained data. A well-developed CRDP system has the advantage of being easily deployed in the field due to its reduced cost, its small size and weight, its optional power supply and the possibility of very quick data collection (Lane, 2000; Rieke-Zapp *et al.*, 2009; Bird *et al.*, 2010; Javernick *et al.*, 2014).

Despite the wealth of available photogrammetric solutions, and the possibility to provide a lightweight and very accurate surveying equipment customized for use by earth scientists, 'potential photogrammetric users continue to have reservations about its potential and often consider its field use to be too complicated' (Rieke-Zapp *et al.*, 2009). In response, this paper presents an example of how CRDP can be used in the field to collect information on fluvial microtopography efficiently and effectively. We tested a recently developed non-proprietary CRDP technique (Bertin *et al.*, 2015), for which the imaging system relies on two consumer-grade digital cameras, in a field environment, measuring exposed gravel bars at the grain scale. A small meandering gravel-bed river in New Zealand was the location for the tests. Imagery data were collected at three distinct gravel bars, allowing testing in a variety of sediment size and surface structure settings. A ground-truth object was used on site to assess the accuracy of obtained elevation data, generally performed in other studies using an independent measuring device. CRDP readily produced sub-millimetre resolution and accuracy DEMs, without the need to deploy control targets on the riverbed for calibration. Using CRDP has the advantage that calibration of the cameras can be carried out in the laboratory before going to the field. We show that by doing so, DEM collection is not affected negatively with test undertaken on the field site. Information derived from the CRDP data was adequate to monitor surface roughness, grain size and three-dimensional (3D) arrangement. Ultimately, this allowed examination of the sedimentological contrasts between bars within the reach.

Methodology

Study site: the whakatiwai river

Field data were collected from the Whakatiwai River (Figure 1A), located in the North Island of New Zealand (37° 05′ S, 175° 18′ E), a small gravel-bed river flowing over greywacke material and draining a watershed of ~12 km^2 [maximum elevation *c.* 490 m above mean sea level (a.m.s.l.)]. The Whakatiwai is fed by numerous small streams originating from the steep east-facing slopes of the Hunua Ranges, and flows to sea in a very short distance, roughly 10 km from its source to the river mouth in the Firth of Thames. On the valley floor, the Whakatiwai is a meandering river, with rapid alluvium bank erosion during flood flows, which essentially transports cobbles (5–25 cm) and pebbles (1–5 cm), with occasional patches of sand/silt and small boulders found along its bed. Because of its short span, there is no gravel–sand transition; the riverbed remains gravelly all the way through to the river mouth. In terms of hydrologic regime, the Whakatiwai is governed by flashy hydrographs and competent flows during the autumn–spring season, with mostly low flows over the summer months, during which gravel bars become vegetated. No flow gauging exists for the river; hence flow data are unavailable for the site.

For the tests a ~200 m long study reach was chosen, situated only 100 m upstream of the river mouth and comprising numerous well-defined gravel bars adjacent to the eroding banks. Three exposed and vegetation-free gravel bars were selected, covering a range of sediment size and surface structures (Figure 2). They were labelled bar #1 to bar #3, with numbers increasing upstream. Within each bar, a small area of exposed gravel (~0.5 m^2), termed 'patch', was chosen at the bar head close to the water edge, for consistency in the measurements, also ensuring the surfaces studied are regularly water-worked.

CRDP deployment and field DEM collection

Imagery data were collected from the three patches in August 2014, after an extended period of dry weather, following a methodology developed in the laboratory and presented in Bertin *et al.* (2015). The two cameras used in stereo (side-by-side, separated by a 250 mm baseline distance between the two optical centres) were Nikon D5100s [16.2 Mpixel complementary metal oxide semiconductor (CMOS) sensors] with Nikkor 20 mm lenses. The cameras, fully charged, were rigidly attached on a 1.2 m long mounting bar that could be hanged horizontally (using a bubble level) above the riverbed using two tripods (Figure 1B). The setup (cameras, tripods and mounting bar) weighed approximately 8 kg.

Prior to transport to the field, the cameras' arrangement on the mounting bar was carefully calibrated in the laboratory by recording stereo photographs (also called stereoscopic images) of a flat chequerboard, and using Bouguet's (2010) Matlab® toolbox to determine the calibration parameters [readers should refer to Bertin *et al.* (2015) for a complete description of the calibration process]. The aperture was set to f/20, ensuring a large depth of field, and focus was set at a distance of 0.8 m, based on the expected field requirements. After calibration, care was taken to ensure that the cameras' arrangement (i.e. relative rotation and translation) was not disturbed.

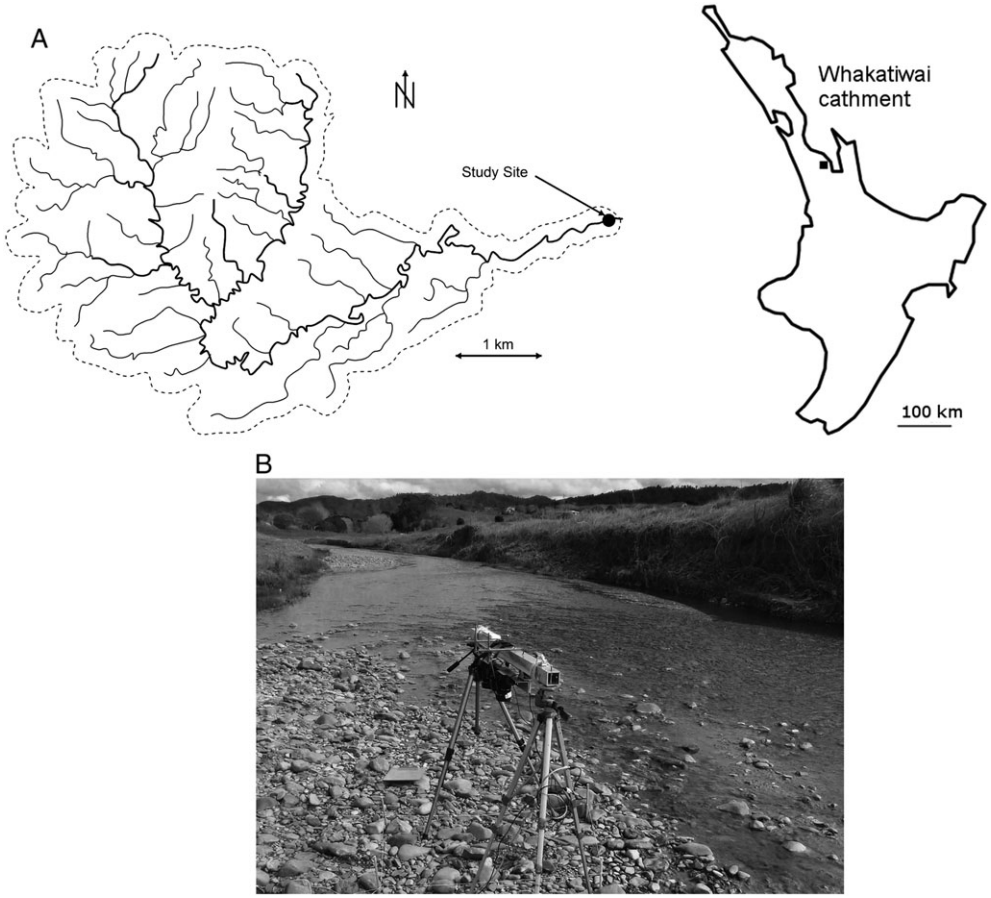

Figure 1. Whakatiwai catchment in the North Island of New Zealand. (A) Site location. (B) Image of CRDP deployment on bar #2, looking upstream. Note the alignment of the setup with the apparent flow direction.

Subsequent testing in the field, after transport, confirmed that minimal disturbance occurred.

Whilst in the field, we attempted to orientate the mounting bar parallel to the antecedent flow direction (Figure 1B), determined by eye from channel shape, producing photographs and DEMs with *x*-axis values increasing downstream (e.g. Figure 3). This later allowed to relate the measured bed properties to the local flow direction. Stereo photographs of the exposed patches were recorded vertically, reducing occlusions (i.e. shadowed areas that cannot be seen in one or the two images) on the surface compared with oblique measurements, from a height of approximately 0.8 m, resulting in point data spacing (i.e. pixel size) ~0.2 mm and a theoretical depth resolution ~0.6 mm. Cameras were operated in manual mode, with the possibility to vary the shutter speed to have well-illuminated and contrasted photographs necessary for successful stereo matching (Bertin *et al.*, 2015). Remote control was possible by connecting the cameras to a laptop.

Data processing consisted in rectifying the stereo photographs to epipolar geometry using the calibration parameters, and transforming the images with the multi-scale Retinex algorithm in GIMP®, before pixel-to-pixel stereo matching using Gimel'farb's (2002) SDPS, providing point cloud data and ortho-images. Because the SDPS algorithm matches corresponding points along lines of one pixel width, accurate image rectification (hence accurate calibration) is essential to produce stereo photographs whose corresponding pixels are ideally on the same scanline (also called epipolar lines, i.e. same vertical position in a photograph). Doing so minimizes the systematic matching errors due to calibration. Image transformation with Retinex heightens the similarity between the two images forming a stereo photograph and improves stereo-matching performance (Bertin *et al.*, 2015), which is specifically important in the field application lacking direct control over the illumination. From the point cloud data, DEMs were interpolated onto regular grids with 1 mm spacing, first by interpolating onto 0.25 mm grids, consistent with the best resolution achievable, to minimize the loss of topographic information (Hodge *et al.*, 2009b; Bertin *et al.*, 2014), then resampling onto the final grids to expedite calculations with minimal surface smoothing [mean unsigned (absolute) error, MUE ~0.025 mm and standard deviation of error, SDE ~0.035 mm between initial and resampled surfaces]. Before resampling onto a 1 mm grid, outliers were identified using the mean elevation difference parameter (Hodge *et al.*, 2009b), and replaced in the DEMs using bi-cubic spline interpolation. Because the MUE between original and filtered DEMs accounted for less than 0.01 mm, filtering was considered optional and its application was not stringent.

CRDP validation and field DEM accuracy

CRDP data quality assessment was done in two ways, by (i) checking on site the validity of the calibration performed in the laboratory prior to moving to the field; and (ii) measuring a ground-truth object, to realistically determine the accuracy of the field DEMs.

To ascertain the validity of the calibration performed in the laboratory, after having transported the CRDP setup to the field, a small chequerboard (0.3 m × 0.2 m, ~0.2 kg, made of alternating black and white squares) was placed on the riverbed and photographed in different positions, altogether covering the common field of view (CFoV) between both cameras. The

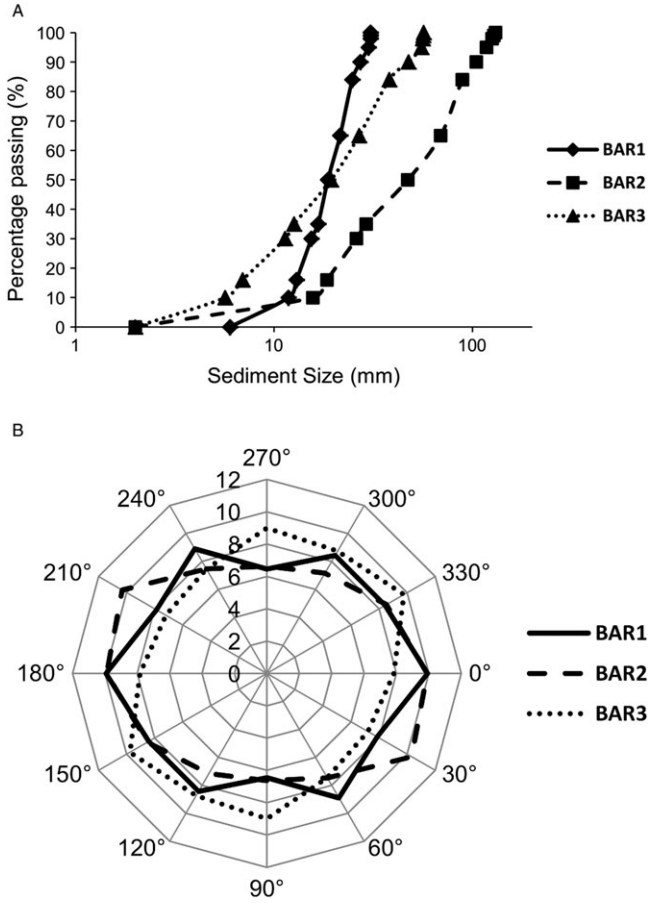

Figure 2. (A) Bed-surface grain-size distributions for the three Whakatiwai patches. (B) Frequency distributions of the *a*-axis (i.e. long axis) orientation of the grains with respect to the flow direction determined by eye in the field (from 0° to 180°).

stereo photographs were rectified using the calibration data obtained in the laboratory, and the rectification error, which is the absolute scanline difference between corresponding pixels (Bradley and Heidrich, 2010; Bertin *et al.*, 2015), was measured for every corners of the squares in all rectified stereo photographs of the chequerboard (i.e. at about 200 locations throughout the measurement area). The mean, standard deviation, and maximum rectification error were computed, and compared with values obtained before moving to the field.

Final DEM quality was assessed by measuring a 3D-printed gravel bed, specifically transported to the field, following the method of Bertin *et al.* (2014). The use of this realistic ground-truth object of a water-worked gravel bed improves on previous DEM assessment methods, traditionally requiring check points to be deployed on the riverbed and surveyed with a total station, to be able to compare with the measurements after co-registration of the two (Butler *et al.*, 1998; Lane, 2000; Lane *et al.*, 2000; Bouratsis *et al.*, 2013), in terms of density/repartition of the check points and registration errors, hence reliability of the assessment. We show herewith that the field use of the 3D-printed gravel bed ground truth sped up and made DEM quality assessment easier. For the assessment, the 3D-printed gravel bed model (296 mm × 184 mm, ~1.5 kg, shown in Figure 4) was imaged with CRDP besides gravel-bar microtopography (same camera distance of 0.8 m). After DEM reconstruction, measured elevations were aligned with the 'truth' elevations and compared at more than 800 000 points, located every 0.25 mm on an orthogonal grid, to realistically determine the field performance of CRDP in this work.

DEM analysis and information on gravel-bar surface structure

Before the DEMs were analysed, it was necessary to remove the combined effect of the local bed slope and setup misalignment from the riverbed (i.e. non-parallelism), which could obscure smaller grain-scale properties. In the absence of bedforms, linear trend surfaces were removed from the DEMs using a least-squares fit procedure (Aberle and Nikora, 2006; Cooper and Tait, 2009; Hodge *et al.*, 2009a), and DEMs were normalized to have a mean elevation equal to zero.

Analysis of gravel-bar topography and surface structure started with the calculation of first-order moments of detrended bed elevations: the range (Δ_Z), standard deviation (σ_Z) and skewness (S_k) were evaluated. The first two parameters are surrogates of grain roughness parameters based on sediment size (Nikora *et al.*, 1998; Aberle and Smart, 2003; Entwistle and Fuller, 2009; Heritage and Milan, 2009). The bed elevation skewness is useful to determine if a gravel bed is water-worked, in this case displaying positive values, contrasting with the negatively skewed man-made screeded gravel beds (Aberle and Nikora, 2006). Generalized two-dimensional (2D) second-order structure functions (Nikora *et al.*, 1998), similar to using semivariograms, were used to estimate the correlations between detrended elevations at different lags and in different directions. DEM analysis continued with the evaluation of the slope and aspect angles of each of the 1 mm^2 DEM grid cells (Hodge *et al.*, 2009a), providing information on grain arrangement at the bar surface. The last step in our investigation of DEM properties was the evaluation of the inclination index, representing particle imbrication, which should be maximal in the direction of the flow (Laronne and Carson, 1976), by analysing the signs of elevation changes between successive pairs of DEM points at different lags and in different directions, following the method presented in Millane *et al.* (2006). Information on how to use these different statistical analysis methods applied to the DEMs is introduced in detail in the references provided, and thus is not repeated herewith.

Image analysis and information on bed-surface grain size and orientation

To complement information derived from the DEMs, grain-size distributions (GSDs) based on the sediment grains' intermediate (*b*-) axis, and the grains' long (*a*-) axis orientation, were determined using the image-analysis tool Basegrain®, which allows for automatic grain separation in digital pictures of gravel beds and applies Fehr's (1987) line-sampling method for the analysis of the results (Detert and Weitbrecht, 2012). For each patch, a single photograph collected with CRDP was necessary.

In order to determine the bed-surface composition (and not the subsurface composition, as per default), the percentage of non-detected fines at 10 mm was changed from 25% to 10% during the analysis of the results, as in Rüther *et al.* (2013). Moreover, the ratio of image-detected *b*-axis (written *b*′) and true *b*-axis, which generally differs from unity due to particle burial, foreshortening and overlapping (Graham *et al.*, 2010), was adjusted to obtain GSDs comparable with GSDs obtained by manual size-sieving. Thus, $b/b' = 1.19$, a value also reported from armour layers formed in a laboratory flume (Bertin and Friedrich, submitted for publication). Grain orientation was automatically determined by fitting an ellipse, whose areal normalized second-central moment equals that

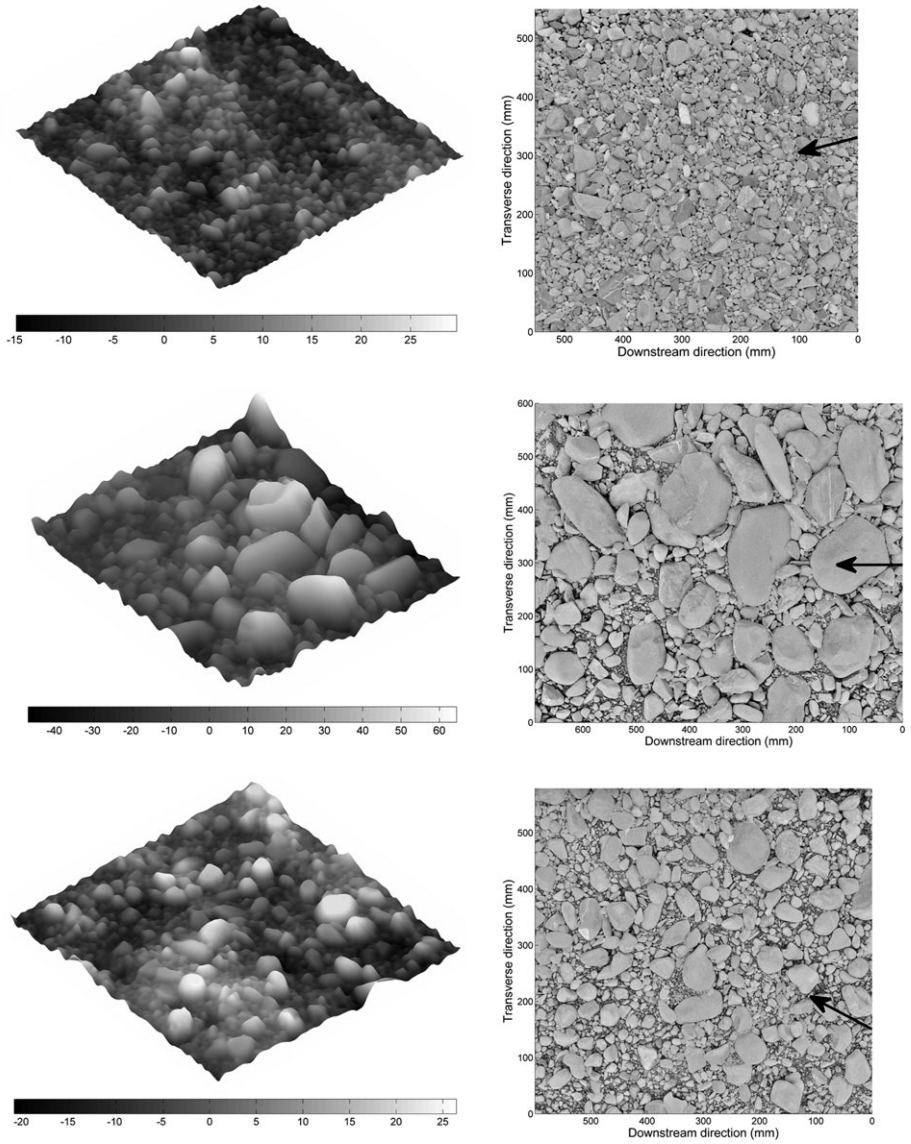

Figure 3. Final DEMs and ortho-images from the Whakatiwai patches (bar #1 to bar #3 from top to bottom). Elevation is represented as gradient of greys, and is in millimetres. Flow direction, determined visually in the field, is from right to left. Arrows show the most probable flow direction (Figure 8).

of the grain, and by computing the angle formed between the ellipse long axis and the flow-orientated image long axis.

Field Observations and Analysis

Bed-surface grain size and orientation

The three patches examined present large differences in sediment size at the bar surface (Figures 2A and 3). The median sediment size (D_{50}) varied between 18 and 47 mm; D_{16} between 7 and 18 mm; and D_{90} between 27 and 104 mm. The patch in bar #1 was the better sorted of the three patches, with a geometric standard deviation $\sigma = \sqrt{D_{84}/D_{16}} = 1.4$, compared with 2.2 and 2.4 for bar #2 and bar #3, respectively. Grain-size variability between gravel bars in the same river reach is not surprising (e.g. Verdú *et al.*, 2005; Hauer *et al.*, 2014). Grain-size variability within bars was also recognized, with coarser material found at the bar head compared to the bar tail [D_{50} increased by 30% in average (Rice and Church (2010)]. Despite that consistent patch selection at the bar head was not easily achieved in practice, the between-bar grain-size differences observed in Figure 2A largely exceed the in-bar variability observed by Rice and Church (2010), indicating a neat grain-size difference between bars in the Whakatiwai that is not the result of downstream fining only. It is assumed that this difference arises from a combination of factors, such as the elevation of the patch with respect to the mean water-surface level, the planform position of the gravel bar, consistent with competence considerations (Rice and Church, 2010), and the chute of sediment from the eroding banks.

Grain orientation at the bed surface also differed between patches (Figure 2B). For bar #1, the bed material preferentially aligned its long axis parallel to the flow direction. This preferential alignment of the grains with water-working, linked to an *in situ* reworking of grains in below entrainment threshold conditions, was observed previously (Butler *et al.*, 2001; Aberle and Nikora, 2006). For bar #2, the same preferential alignment of the grains was observed, but this time, the proportion of grains forming a 30° angle to the flow with their *a*-axis was as large as the proportion of grains aligned parallel to the flow. This may suggest that the actual surface-forming flow direction was somewhere between 0° and 30° with respect to the image orientation. The latter analysis should be taken with caution however, as previous research showed that prevailing grain

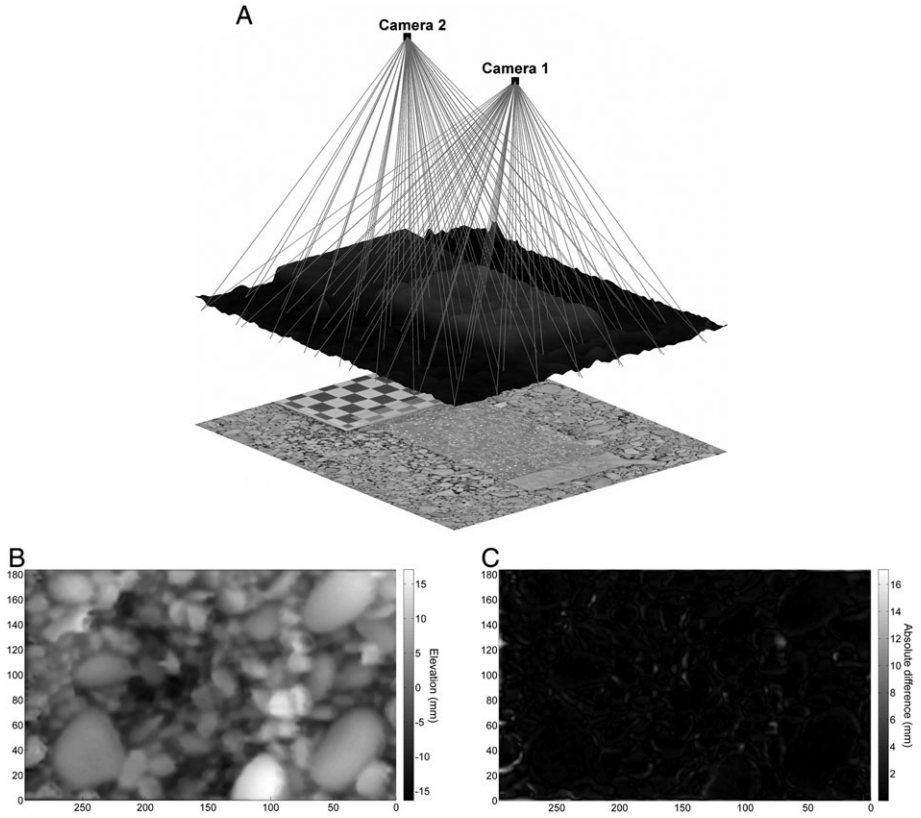

Figure 4. (A) Close-up presentation of on-site quantitative evaluation of CRDP performance using a 3D-printed gravel-bed model. (B) Measured DEM of the 3D-printed model. (C) DEM of difference (DoD) between measured and truth data (0.25 mm sampling distance).

orientation is also influenced by the sediment transport mode, hence is an ambiguous descriptor of flow direction (Hodge *et al.*, 2009a). For instance, coarse grains transported by rolling or sliding often come to rest with their *a*-axis perpendicular to the flow direction (Laronne and Carson, 1976). Bar #3 presents the largest proportion of grains aligned perpendicular to the (assumed) flow direction. There are two possibilities to explain this tendency: the flow direction was not correctly determined; or, more coarse grains were transported by rolling or sliding during the last competent event(s) compared to the other patches.

Grain-scale DEMs and Ortho-images

CRDP naturally produces 2D (i.e. ortho-images) and 2.5D (i.e. DEMs) maps of the surfaces studied (Figure 3). In previous studies, visualization of the ortho-images, and comparison with the DEMs, was considered an effective way of controlling photogrammetric performance qualitatively (Butler *et al.*, 1998; Lane, 2000). Since visual inspection of the ortho-images obtained during this work show high quality (Figure 3), without apparent mixed pixels and/or distortions, we can assume that stereo matching performed well for the entire measurement area.

Field studies using TLS also require imagery data to be collected, whether it is for documenting (Heritage and Milan, 2009) and/or for grain-size analysis (Hodge *et al.*, 2009a). As CRDP data are obtained from imagery, both the DEMs and the ortho-images are automatically referenced within the same coordinate system (Figure 3), which saves the need to align the two.

CRDP validation and DEM accuracy

The rectification error just after calibration (i.e. in the laboratory) was represented by a mean of 0.09 pixel, a standard deviation of 0.08 pixel and a maximum of 0.37 pixel, ensuring minimal systematic error during stereo matching. After moving the CRDP setup to the field, the rectification error increased (mean = 0.29 pixel, standard deviation = 0.23 pixel and maximum = 0.91 pixel), certainly caused by the transport (and shaking that occurred) in the car. It is noted that no particular measure was taken to transport the setup; other than it being placed flat in the boot of the car, surrounded by soft material to protect the equipment and hinder any movement. Despite the increased rectification error, which naturally will affect stereo-matching performance, the rectification error remained below one pixel throughout the imaging area, the threshold above which stereo-matching errors become inevitable, since the SDPS stereo matching is performed along lines of one pixel width. In the case of significantly impacted camera arrangement, which would have prevented accurate image rectification, it would have been possible to re-calibrate on-site using the chequerboard (taking approximately 30 minutes), and/or upon return to the laboratory given sufficient camera battery life.

Figure 4A shows the 3D-printed gravel-bed model used for *in situ* DEM quality assessment. The chequerboard was used to ensure that the 3D model was placed as horizontal on the ground as possible, facilitating the numerical co-registration of measured and truth data (Bertin *et al.*, 2014). Figure 4C shows the DEM of difference (DoD), obtained by differentiating the measured DEM of the 3D-printed model (Figure 4B) with the truth DEM, after alignment of the two. Comparison was done on a grid with 0.25 mm spacing; hence at more than 800 000 locations. Visually, large errors (>10 mm) are rare and are essentially visible at the grains' edges and the troughs of the surface. The measurement of occlusions is a well-known difficulty for both CRDP and TLS (Chandler *et al.*, 2005; Hodge *et al.*, 2009b; Bouratsis *et al.*, 2013; Bertin *et al.*, 2015). Consequently, a general reduction in pore depth and DEM properties such as σ_Z is expected. Quantitatively, most of the measured

DEM points (98%) were within ±3 mm from the truth data, 82% were within ±1 mm, and 58% were within ±0.5 mm. Thus, σ_Z measured from the DEM was 99.8% of the truth value, showing that surface roughness is reliably measured. From the DoD, a MUE of 0.67 mm between measured and truth values was estimated, with a SDE of 1.16 mm and a maximum unsigned error of 17.1 mm. This is not as good as what can be achieved with CRDP in a laboratory setting (MUE = 0.43 mm, SDE = 0.62 mm and maximum unsigned error of 8.16 mm), with a measuring distance of 640 mm and a 250 mm baseline between the cameras (Bertin *et al.*, 2014). We assume that the deterioration in field DEM quality compared with the laboratory is essentially the result of the increased camera-to-object distance used for image recording, hence degraded horizontal and depth measurement resolutions, and the increased rectification error due to transport. However, this evaluation shows that CRDP can measure exposed fluvial surfaces in the field with sub-millimetre resolution and vertical accuracy (based on MUE), and guarantees reliable grain-scale roughness information from the DEMs. CRDP can even outperform TLS, for which a rigorous past application was constrained by the 4 mm laser footprint and resulted in a minimum SDE of ~1.3 mm, after averaging three repeat scans of a plane surface in the laboratory (Hodge *et al.*, 2009b).

DEM analysis

Figure 5A shows the distribution of (detrended) bed elevations for the three patches. All distributions are positively skewed (S_k = 0.71, 0.53 and 0.52, for bar #1 to bar #3, respectively), confirming water-worked gravel surfaces (Aberle and Nikora, 2006). Analysis of the bed-elevation distributions shows that the three patches are different however, and certainly echoes the grain-size differences identified earlier (Figures 2 and 3). Previous studies observed relationships between σ_Z and grain size, generally expressed as D_{50} (Smart *et al.*, 2004; Aberle and Nikora, 2006; Hodge *et al.*, 2009a). Here, bar #1 had the smallest D_{50} and the smallest σ_Z, whilst bar #2 had both the largest D_{50} and σ_Z (Figure 5B). However, the ratio of σ_Z to D_{50} (0.32–0.46) varied between patches, suggesting that D_{50} is not the only factor determining σ_Z, and other factors such as sediment sorting are also responsible (Figure 5C). We found that the ratio D_{50}/σ_Z decreases with the sediment sorting. This suggests that for similar values of D_{50}, poorly-sorted sediments can create more irregular and rougher surfaces, with accentuated grain packing, than well-sorted sediments, which agrees with observations made by Hodge *et al.* (2009a).

Generalized second-order structure functions of (detrended) bed elevations were calculated for all patches for lags up to ±150 mm (corresponding to 3 to 8 D_{50}, depending on the patch), being always larger than the maximum grain size and enough to reach the saturation region, normalized by the saturation level $2\sigma_Z^2$, and plotted as 2D isopleth maps (Figure 6). Similar to previous work (e.g. Aberle and Nikora, 2006), we found that at small lags (up to 1 D_{50}), the surface structure of the gravel bars is isotropic, as shown by the circular contours in the centre of the isopleth maps. The high correlation between pairs of points at small lags is because the elevation pairs used to calculate the structure functions belong likely to the same grain, and this suggests that small grains have no prevailing orientation. As the lag increases, the contours generally become elliptical and supposedly reflect the dominant grain orientation, with the long axis of the ellipse representing the *a*-axis alignment (Nikora *et al.*, 1998; Hodge *et al.*, 2009a), until at large lags, equal to 2 to 5 D_{50} depending on the patch, the contours become very irregular. Bars #1 and #2 both show

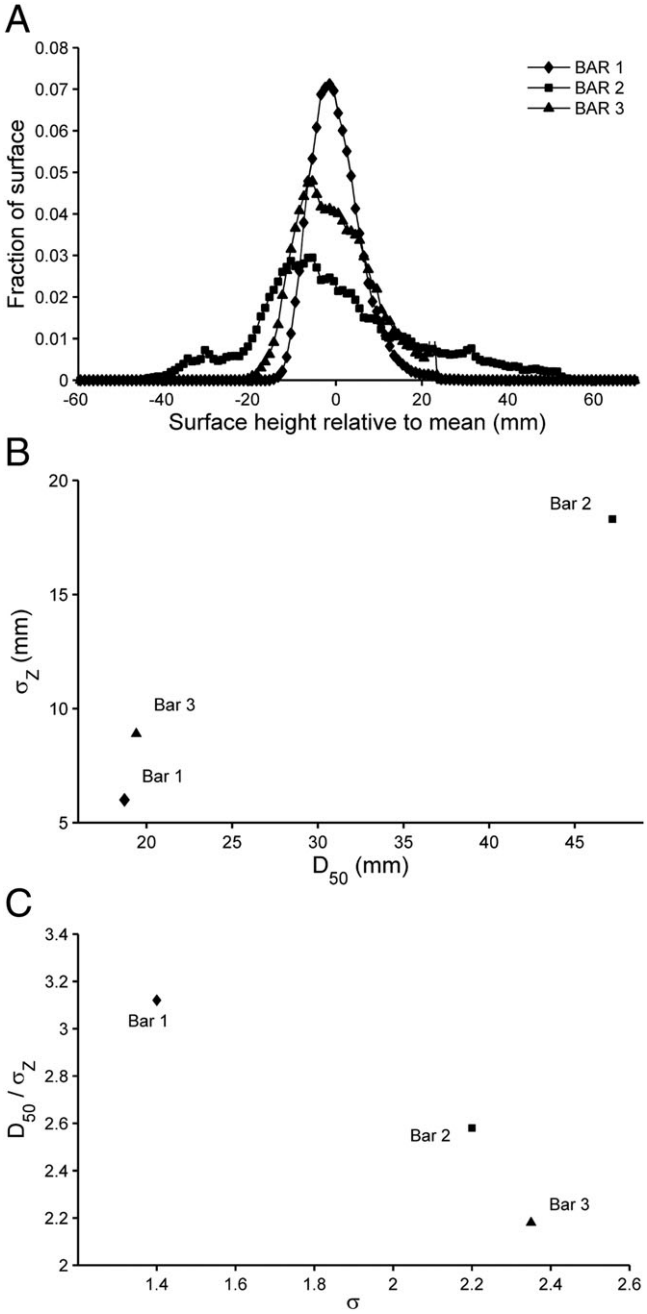

Figure 5. (A) Distributions of surface elevations for the three patches. (B) Relationship between the standard deviation of bed elevations (σ_Z) and the bed-surface D_{50}. (C) Relationship between D_{50}/σ_Z and the sediment geometric sorting (σ).

a dominant grain orientation with the *a*-axis parallel to the flow direction. For both patches, the streamwise correlations are stronger than the cross-flow correlations, and remain strong over scales extending over the streamwise size of the plots. This indicates gravelly structures longitudinal to the flow, a common occurrence for water-worked gravel beds in both the laboratory and the field (Butler *et al.*, 2001; Aberle and Nikora, 2006; Cooper and Tait, 2009; Hodge *et al.*, 2009a; Mao *et al.*, 2011). This observation can be attributed to sediment deposition after contact with the upstream front of a stable grain and particle imbrication. Bar #3 presents a different shape of structure function for lags up to 2 to 3 D_{50}. This may reflect diamond-shape clusters (Aberle and Nikora, 2006; Mao *et al.*, 2011), whose extensive presence can be noticed on the ortho-image (Figure 3), unlike other patches.

The combined distributions of DEM cell slope and aspect angles (Figure 7) show that all three patches have a dominance of

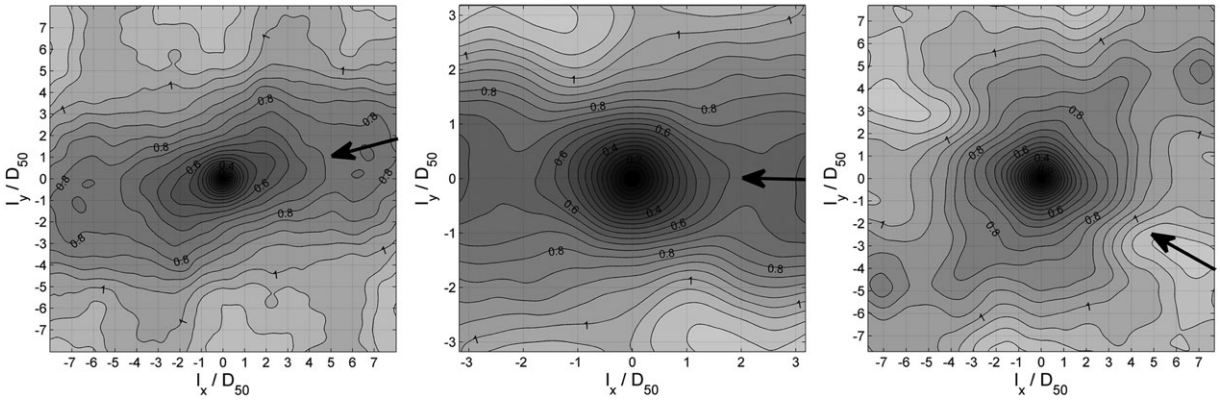

Figure 6. Two-dimensional isopleth maps of the generalized second-order structure functions for the three patches (bar #1 to bar #3 from left to right). The assumed flow direction is along the horizontal axis. Arrows show the most probable flow direction, based on Figure 8.

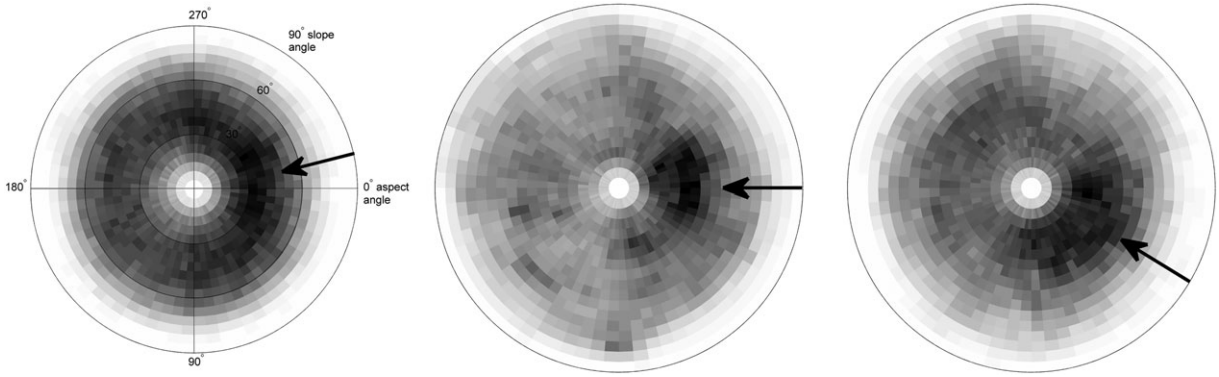

Figure 7. Polar plots of all 1 mm^2 DEM grid cells aspect and slope angles for the three patches (bar #1 to bar #3 from left to right). Aspect angle is from 0° to 360° and slope angle is from 0° to 90°; plots are shaded by point density (high density in black, zero density in white). The assumed flow direction is from 0° to 180°. Arrows show the most probable flow direction, based on Figure 8.

DEM cells with upstream aspects (i.e. aspect angle around 0°). The latter is known to represent particle imbrication (Hodge *et al.*, 2009a), which naturally occurs in a direction parallel to the flow (Laronne and Carson, 1976; Millane *et al.*, 2006). Hence, bar #2 certainly presented the highest rate of surface imbricated grains. From the dominant slope angles in Figure 7, the angle of imbrication is estimated at between 25° and 50° for all patches. The three patches however present different grain arrangements at the bed surface. Bar #1 is characterized by DEM cell slopes rarely exceeding 70° and particle imbrication not as pronounced as on bar #2. Bars #2 and #3 have DEM cells with slope angles sometimes reaching 80°–90°, indicating more packed particles and rougher surfaces, verifying previously presented observations (Figure 5). Bar #3 shows imbrications over a range of directions, from 0° to 90° with respect to the assumed flow direction. Since imbrication is not centred on zero, which means that surface grains predominantly imbricated in directions different from the flow direction, it might suggest that the flow direction was incorrectly determined in the field. Concurrently, imbricated particles covering a range of directions might say that the flow direction changed over the duration of the last competent event, for example varied with flow depth, or that different flows (with different directions) imbricated particles in different ways over time, something which was observed in the past (Millane *et al.*, 2006).

Figure 8 shows the directional inclination indices calculated from the DEMs. Bar #2 shows the largest inclination index; hence, more of the patch area was covered by imbricated particles than on the other patches. This corroborates observations made on the combined distributions of DEM cell slope and aspect angles (Figure 7). For bar #2, the inclination index clearly peaks in the direction of the flow, suggesting the flow direction was correctly determined in the field (Millane *et al.*, 2006). Bar #3 has an inclination index that plateaued for angles between approximately 0° and 90°, which again follows observations made previously on Figure 7. The maximum inclination index for bar #3 is attained for a DEM direction forming a 30° angle with the flow, suggesting that the assumed flow direction was erroneous by 30° (Millane *et al.*, 2006). If this really is the case, the distribution of DEM cell slope and aspect angles (Figure 7) for bar #3, which initially differed from the other

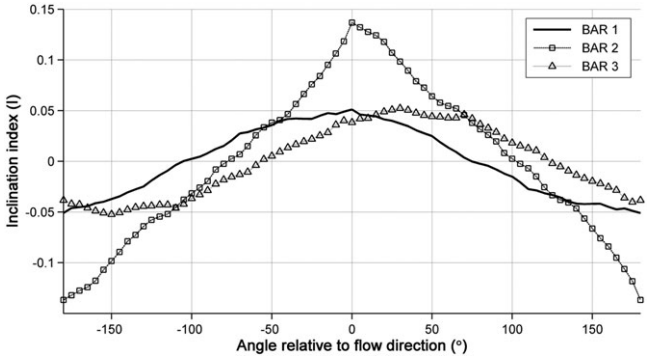

Figure 8. Directional inclination indices for the three patches. Inclination was calculated for all angles between −180° and 180° at a 5° interval, using a separation distance between pairs of points of 1 mm, which is the DEM sampling distance, the lag for which imbrication was the most perceptible.

two patches, would have a more natural look and would exhibit a dominance of DEM cells with upstream aspects, hence particle imbrication in the direction of the flow. Likewise, this would affect the measured frequency-distribution of grains' *a*-axis orientation (Figure 2B), which would then peak for angles perpendicular to the flow direction, indicating a dominance of particles reposing across the flow; and the shape of the 2D structure function (Figure 6), which would also show a dominant ellipse orientation transverse to the flow direction at medium lags. The latter two observations demonstrate that more particles were aligned transverse to the flow on bar #3 than on the other patches, which can be associated with bedload transport mode by rolling and sliding motion (Laronne and Carson, 1976). Bar #1 shows a smoother distribution of inclination indices, skewed to the left of the plot, which might say that the actual surface-forming flow direction is slightly offset from the assumed flow direction. Whilst this is not as clear as on bar #3, this corroborates observations made on Figures 6 and 7.

Discussion

We previously reported on our development of a non-proprietary CRDP technique, making use of consumer-grade digital cameras and off-the-shelf calibration and stereo matching engines, capable of recording gravel beds, water-worked in a laboratory flume, at the grain scale, characterized by sub-millimetre DEM resolution and accuracy (Bertin *et al.*, 2015). We also showed that the same CRDP technique can be used for through-water recording (Bertin *et al.*, 2013). Here, we tested the possibility to deploy the setup and adapt the methodology for measurements in a natural river environment in the field.

CRDP recommended measurement workflow and field potential

Compared with previous fluvial applications of digital stereo photogrammetry, calibration was performed in one go with a chequerboard, and did not require the placement of fixed control targets on each patch, which in turn would require surveys with a total station (or another independent device) for bundle adjustment. In addition to speeding up data collection and limiting the resources needed on site, calibration with a chequerboard prevents the introduction of additional errors due to the total station, which adversely affects calibration, and hence DEM quality (Carbonneau *et al.*, 2003). It is noted, however, that having fixed control targets of known coordinates [e.g. using a global positioning system (GPS) tracker] (i) allows to place measured DEMs within a global coordinate system, (ii) obviates the need to remove trend surfaces (see earlier section on 'DEM analysis and information on gravel-bar surface structure') and (iii) allows direct surface differencing in sequential surveys, which, however, is deemed unnecessary for small-scale DEMs. For this fieldwork, the application of photogrammetry was rendered even more effective by doing the calibration in 'ideal' conditions in the laboratory, providing optimum calibration parameters, prior to moving to the field. There are drawbacks to this method however. The arrangement of the cameras on the mounting bar, after calibration, needs to remain as unmodified as possible until the gravel-bed images are collected, to guarantee representative calibration parameters. Using a chequerboard allowed efficient and effective testing of the calibration validity after transport to the field, which was confirmed in this study. Moreover, a laboratory calibration requires pre-supposition of the camera-to-riverbed and baseline distances used in the field, both controlling the measurement performance, and therefore limiting the applicability of the calibrated setup to a range of tasks (microtopographic measurements herewith). With the large body of work on the subject, it is well known that digital cameras are versatile instruments, able to perform 3D measurements over a range of spatial scales, from microtopography to channel shape (Lane, 2000; Butler *et al.*, 2001; Lane *et al.*, 2003; Javernick *et al.*, 2014). The studied scale will depend on the application details. Our CRDP workflow can accommodate various measurement scenarios: (i) several overlapping small-scale DEMs can be merged together, producing a larger DEM that shares the measurement quality of the original DEMs (Bertin *et al.*, accepted for publication); (ii) the CRDP setup can be adjusted and recalibrated on site to suit larger-scale measurements better (e.g. by increasing the baseline and camera distance); (iii) more than one pre-calibrated setup can be transported to the field, each attributed a specific task; and (iv) a camera can be detached to collect imagery from which larger-scale DEMs are reconstructed using other methods than herewith presented (e.g. SfM, Javernick *et al.*, 2014). It is noted that novel SfM/MVS photogrammetric techniques, using a single non-calibrated camera, may provide a viable alternative to classical stereo photogrammetry in measuring gravel patches at fine scales. Some SfM/MVS pipelines are freely available (Stumpf *et al.*, 2015). They are able to generate data at high resolution (James and Robson, 2012) and can begin to tackle the problem of occlusions since imagery is collected from different viewpoints. However, SfM/MVS-generated DEMs may suffer from large non-linear distortions due to inadequate lens distortion calibration (Fonstad *et al.*, 2013; Ouédraogo *et al.*, 2014), a drawback that has been resolved in traditional stereo photogrammetry (Wackrow and Chandler, 2008; Bertin *et al.*, 2015). Furthermore, a large number of images (possibly hundreds) are necessary to reach DEM densities comparable to the one required for this study, and will result in much longer processing time (James and Robson, 2012).

In conjunction with accurate calibration, scanline-based pixel-to-pixel stereo matching adopted in this study resulted in dense DEMs, with the possibility to have a DEM grid size as small as the pixel size at the distance of the riverbed. This fact limited surface smoothing and improved on traditional area-based methods, whereby the smallest DEM grid size is chosen to be five times the pixel size on the surface (Lane *et al.*, 2000). Limited post-processing was applied on the DEMs, which was deemed optional and prevented the introduction of new errors. For TLS applications, measurement resolution can also be a limiting factor for DEM quality. Hodge *et al.* (2009a, 2009b) reported using a laser-scanning system with a 4 mm footprint in a field study measuring grain-scale fluvial morphology. A rigorous methodology was necessary to maximize point coverage and density and to minimize the effect of the oblique scan angles, by collecting data from two or three scanner positions around each patch, registered together by simultaneously scanning a network of fixed targets, and taking three repeat scans from each scanner position to minimize errors in the data. The reported turn-round time was approximately 25–30 minutes per scan. However, there was still the need of significant post-processing in the form of three filters to obtain accurate metrics (Hodge *et al.*, 2009a, 2009b; Smith *et al.*, 2012).

A potential advantage of TLS over CRDP is its direct 'time-of-flight' measurement, compared with measurements relying on image quality and texture (Hodge *et al.*, 2009b). This certainly helped promote the advent of range (also called time-of-flight) cameras and usage in the Earth Sciences (Mankoff and Russo, 2013; Nitsche *et al.*, 2013). However, a number of difficulties, including the need to collect data in low-light conditions,

currently limit the applicability of this recent technology in the field and prevent accurate grain-scale data collection. Moreover, surface reflectivity can introduce systematic time-of-flight measurement errors (Hodge *et al.*, 2009b; Nitsche *et al.*, 2013), for which the only remedies are repeat scan processing and filtering. In contrast, digital photogrammetry provides the opportunity to optimize image collection (e.g. by varying the shutter speed), and use image transformation techniques, such as Retinex, to improve stereo matching. This proved to be a source of significant DEM accuracy improvement in the laboratory (Bertin *et al.*, 2015), and we expect this will become even more important in the field, where lighting conditions are variable.

During this fieldwork, we also tested the possibility to assess DEM quality without ground check points and a total station. Data quality assessment, an important component to every topographic survey (Lane *et al.*, 2005), was performed using a ground-truth object produced by 3D printing (Bertin *et al.*, 2014). Due to the small size of the 3D-printed model, we believe this assessment suits small-scale DEMs well, but would not be adequate for larger DEMs. In addition to saving time on site, the use of a realistic ground truth provided a precise and reliable quantification of DEM errors. This way, we showed that CRDP is capable of measuring complex surfaces in the field with good vertical accuracy.

Riverbed morphology and between-bar variations

A range of methods was used to analyse the gravel-bed DEMs, some of which are by now well-known to the Earth Science community (e.g. probability distribution functions and generalized structure functions), and have been used extensively in studies on the geomorphology of gravel-bed rivers over the past decades (e.g. Robert, 1991; Butler *et al.*, 2001; Aberle and Nikora, 2006). Other methods however, such as the combined distribution of slope and aspect angles of the DEM cells and the directional inclination index, have only been used in a handful of studies on gravel-bed rivers so far (Millane *et al.*, 2006; Hodge *et al.*, 2009a; Qin *et al.*, 2012). Analysis of surface elevations (Figure 5) identified differences between the three patches, and showed that both the median grain size (D_{50}) and sediment sorting (σ) exert control on the surface irregularity and geometric roughness after water-work, with the geometric roughness represented by the standard deviation of bed elevations (σ_Z). The bed-elevation distribution skewness (S_k), positive for all bars, confirmed that the patches comprised water-worked gravels (Aberle and Nikora, 2006). Information derived from the 2D structure functions was useful to identify variations on the size, orientation and type of gravel structures found on the gravel bars. Bars #1 and #2 had longitudinal gravel structures, extending over lengths several times the surface D_{50}. Diamond-shaped clusters were observed on bar #3, which was evidenced in the 2D isopleth maps (Figure 6). There was a good agreement between the prevailing grain orientation determined using either the structure functions or grain delineation in the photographs (Figure 2B). However, this failed at being conclusive on the surface-forming flow direction (Hodge *et al.*, 2009a). The latter is notoriously difficult to determine accurately from visual observations in the field (e.g. Smart *et al.*, 2004). Using DEMs has improved means to determine the antecedent flow direction from measurements of exposed gravel surfaces, especially when relying on surface inclinations (Smart *et al.*, 2004; Aberle and Nikora, 2006; Millane *et al.*, 2006). In this study, analyses of the directional inclination index (Figure 8) and the combined distribution of DEM cell slope and aspect angle (Figure 7) reached the same conclusion on particle imbrication, hence surface-forming flow direction(s). Bar #2 was the patch with most of its surface covered with imbricated particles (Figure 8). The neat imbrication in a single direction confirmed the flow direction determined in the field. Bars #1 and #3 presented imbricated particles over a range of directions, suggesting flow direction changed over the last flow event(s) and imbricated particles in different ways. Plotting the directional inclination index has the advantage of clearly showing the angle(s) for which imbrication is the most significant (Millane *et al.*, 2006), hence the surface-forming flow direction(s). Surface slope and aspect is hardly parameterizable, but provides information on the angles with which sediment particles repose at the surface.

As Rice and Church (2010) pointed out, focus in past research has been on bed-material grain size variation in gravel-bed rivers at reach and river-length scales, and has sought to explain the principal features, including downstream fining and the gravel–sand transition. Relatively little information is currently available on the variations in surface structure and geometric roughness, despite that we know that these factors influence flow resistance and sediment transport (Laronne and Carson, 1976; Komar and Li, 1986; Church *et al.*, 1998), and may be used to explain the processes responsible for the formation and evolution of sedimentary units, such as riffles and pools (Hodge *et al.*, 2013). As shown in the presented study, field deployment of remote-sensing techniques, such as CRDP, is becoming easier, and statistical analysis of the DEMs has the potential to provide important information on the variations in surface structure.

Conclusion

Collecting information on gravel-bed rivers at the grain scale in both the laboratory and the field, although technically and methodologically challenging, is important for applications such as roughness studies, sediment transport and the interactions between animals and the geomorphology, topics relevant to many river practitioners. Sediment size and 3D arrangement at the riverbed surface are all useful information to collect; these factors control physical processes such as the resistance to the flow, the ability of the flow to entrain sediment and create sediment structures, which in turn can explain the existence of distinct sedimentary units within a river reach, and the large-scale evolution of river basins.

Along with TLS, CRDP is a mature remote-sensing technique, theoretically capable of high-spatial point density and accuracy, necessary for precisely measuring gravel-bed microtopography. Despite extensive applications in the Earth Sciences, both techniques suffer from a tedious measuring workflow when it comes to measure fluvial sediment at the grain scale, which currently hinders the general applicability of these techniques in the field, and in spite of the best methodological efforts, may not always guarantee reliable findings based on the measured DEMs.

This study presented how CRDP can be efficiently deployed in the field to collect high-resolution and high-accuracy DEMs from exposed gravel bars. The only resources needed were two digital cameras mounted on a rigid bar, two tripods and a laptop. Field data collection was greatly simplified by undertaking the necessary calibration in the laboratory, prior to moving to the field. This removed the need to deploy ground-control targets. Dense stereo matching and image optimization helped the collection of DEMs without being impacted by variable lighting conditions, which challenge applications of TLS and range imaging. A light-weight 3D-printed model, resembling a water-worked gravel bed, was used on site as a ground-truth object to assess the accurate measurement of elevation data. In

this work, DEMs were collected at a 1 mm sampling distance, which could go as low as the pixel size at the distance of the riverbed (i.e. around 0.25 mm), with a measured accuracy of 0.67 mm (based on MUE), which guaranteed reliable grain roughness properties from the DEMs.

A variety of statistical methods was applied to the DEMs and identified between-bar sedimentological contrasts. Analysis of the distribution of surface elevations confirmed that the surfaces were water-worked (positive distribution skewness) and allowed ranking the patches by their geometrical roughness (σ_Z). It showed how σ_Z is influenced by both the median grain size (D_{50}) and sediment sorting (σ). Information derived from the 2D structure functions helped identify variations in size, orientation and type of gravel structures found on the gravel bars. Bars #1 and #2 both had longitudinal gravel structures, which contrasted with the diamond-shaped clusters found on bar #3. The prevailing grain orientation determined from automatically delineated grains in the photographs supported observations from the 2D structure functions, but failed at being conclusive on the surface-forming flow direction. For the latter, analyses of the directional inclination index and the combined distribution of DEM cell slope and aspect angle were the most helpful, showing the direction(s) of particle imbrication, hence the surface-forming flow direction(s).

Continuous progress in topography remote sensing is important to extend our fluvial knowledge, for example by allowing the study of flow-channel processes at different scales, in both space and time. Better characterization of these processes *in situ*, with the efficient and effective measurement of submerged surfaces, is a critical task that needs to be tackled in future, ultimately to develop a technique customized for use by fluvial geomorphologists in the field.

Acknowledgements—The authors would like to thank S. Stähly for assistance in obtaining the field data. The study was partly funded by the Marsden Fund (Grant No. UOA1412), administered by the Royal Society of New Zealand.

References

Aberle J, Nikora V. 2006. Statistical properties of armored gravel bed surfaces. *Water Resources Research* **42**: W11414.

Aberle J, Smart GM. 2003. The influence of roughness structure on flow resistance on steep slopes. *Journal of Hydraulic Research* **41**: 259–269.

Bertin S, Friedrich H. n.d. Submitted for publication. Stable fluvial armors and surface structure replicability. In *Water Resources Research*.

Bertin S, Friedrich H, Delmas P. n.d. Accepted for publication. A merging solution for close-range DEMs to optimise surface coverage and measurement resolution. *Photogrammetric Engineering & Remote Sensing*.

Bertin S, Friedrich H. 2016. A merging solution for close-range DEMs to optimise surface coverage and measurement resolution. *Photogrammetric Engineering & Remote Sensing* **82**: 31–40.

Bertin S, Friedrich H, Delmas P, Chan E. 2013. The use of close-range digital stereo-photogrammetry to measure gravel-bed topography in a laboratory environment. In Proceedings of the 35th IAHR Congress. China: Chengdu.

Bertin S, Friedrich H, Delmas P, Chan E, Gimel'farb G. 2014. DEM quality assessment with a 3D printed gravel bed applied to stereo photogrammetry. *Photogrammetric Record* **29**: 241–264.

Bertin S, Friedrich H, Delmas P, Chan E, Gimel'farb G. 2015. Digital stereo photogrammetry for grain-scale monitoring of fluvial surfaces: error evaluation and workflow optimisation. *ISPRS Journal of Photogrammetry and Remote Sensing* **101**: 193–208.

Bird S, Hogan D, Schwab J. 2010. Photogrammetric monitoring of small streams under a riparian forest canopy. *Earth Surface Processes and Landforms* **35**: 952–970.

Bouguet J.-Y. 2010. http://www.vision.caltech.edu/bouguetj/calib_doc/ [1 July 2014].

Bouratsis P, Diplas P, Dancey CL, Apsilidis N. 2013. High-resolution 3D monitoring of evolving sediment beds. *Water Resources Research* **49**: 977–992.

Bradley D, Heidrich W. 2010. Binocular camera calibration using rectification error. *Proceedings of the 2010 Canadian Conference on Computer and Robot Vision* (*CRV*), Ottawa, Ontario, Canada; 183–190.

Butler JB, Lane SN, Chandler JH. 1998. Assessment of DEM quality for characterizing surface roughness using close range digital photogrammetry. *Photogrammetric Record* **16**: 271–291.

Butler JB, Lane SN, Chandler JH. 2001. Characterization of the structure of river-bed gravels using two-dimensional fractal analysis. *Mathematical Geology* **33**: 301–330.

Butler JB, Lane SN, Chandler JH, Porfiri E. 2002. Through-water close range digital photogrammetry in flume and field environments. *Photogrammetric Record* **17**: 419–439.

Carbonneau PE, Lane SN, Bergeron NE. 2003. Cost-effective non-metric close-range digital photogrammetry and its application to a study of coarse gravel river beds. *International Journal of Remote Sensing* **24**: 2837–2854.

Chandler J, Fryer J, Jack A. 2005. Metric capabilities of low-cost digital cameras for close range surface measurement. *Photogrammetric Record* **20**: 12–26.

Church M, Hassan MA, Wolcott JF. 1998. Stabilizing self-organized structures in gravel-bed stream channels: field and experimental observations. *Water Resources Research* **34**: 3169–3179.

Cooper JR, Tait SJ. 2009. Water-worked gravel beds in laboratory flumes – a natural analogue? *Earth Surface Processes and Landforms* **34**: 384–397.

Detert M, Weitbrecht V. 2012. Automatic object detection to analyze the geometry of gravel grains. *Proceedings of the River Flow 2012*, San Jose, Costa Rica; 595–600.

Du Preez C, Tunnicliffe V. 2012. A new video survey method of microtopographic laser scanning (MiLS) to measure small-scale seafloor bottom roughness. *Limnology and Oceanography: Methods* **10**: 899–909.

Entwistle NS, Fuller IC. 2009. Terrestrial laser scanning to derive surface grain size facies character of gravel bars. In Laser Scanning for the Environmental Sciences. Wiley-Blackwell: Oxford; 102–114.

Fehr R. 1987. *Geschiebeanalysen in Gebirgsflüssen* [*Sediment analysis in mountain rivers*]. Conversion and comparison of various analytical methods. Mitteilungen der Versuchsanstalt für Wasserbau, Hydrologie und Glaziologie, Eidgenössische Technische Hochschule: Zürich; 92.

Fonstad MA, Dietrich JT, Courville BC, Jensen JL, Carbonneau PE. 2013. Topographic structure from motion: a new development in photogrammetric measurement. *Earth Surface Processes and Landforms* **38**: 421–430.

Gimel'farb G. 2002. Probabilistic regularisation and symmetry in binocular dynamic programming stereo. *Pattern Recognition Letters* **23**: 431–442.

Graham DJ, Rollet AJ, Piégay H, Rice SP. 2010. Maximizing the accuracy of image-based surface sediment sampling techniques. *Water Resources Research* **46**: W02508.

Hannam M, Moskal ML. 2015. Terrestrial laser scanning reveals seagrass microhabitat structure on a tideflat. *Remote Sensing* **7**: 3037–3055.

Hauer C, Unfer G, Holzapfel P, Haimann M, Habersack H. 2014. Impact of channel bar form and grain size variability on estimated stranding risk of juvenile brown trout during hydropeaking. *Earth Surface Processes and Landforms* **39**: 1622–1641.

Heritage GL, Milan DJ. 2009. Terrestrial laser scanning of grain roughness in a gravel-bed river. *Geomorphology* **113**: 4–11.

Hodge R, Brasington J, Richards K. 2009a. Analysing laser scanned digital terrain models of gravel bed surfaces: linking morphology to sediment transport processes and hydraulics. *Sedimentology* **56**: 2024–2043.

Hodge R, Brasington J, Richards K. 2009b. In situ characterization of grain-scale fluvial morphology using terrestrial laser scanning. *Earth Surface Processes and Landforms* **34**: 954–968.

Hodge RA, Sear DA, Leyland J. 2013. Spatial variations in surface sediment structure in riffle–pool sequences: a preliminary test of the Differential Sediment Entrainment Hypothesis (DSEH). *Earth Surface Processes and Landforms* **38**: 449–465.

James MR, Robson S. 2012. Straightforward reconstruction of 3D surfaces and topography with a camera: accuracy and geoscience application. *Journal of Geophysical Research, Earth Surface* **117**: F03017.

James TD, Carbonneau PE, Lane SN. 2007. Investigating the effects of DEM error in scaling analysis. *Photogrammetric Engineering & Remote Sensing* **73**: 67–78.

Javernick L, Brasington J, Caruso B. 2014. Modeling the topography of shallow braided rivers using structure-from-motion photogrammetry. *Geomorphology* **213**: 166–182.

Komar PD, Li Z. 1986. Pivoting analyses of the selective entrainment of sediments by shape and size with application to gravel threshold. *Sedimentology* **33**: 425–436.

Lane SN. 2000. The measurement of river channel morphology using digital photogrammetry. *Photogrammetric Record* **16**: 937–961.

Lane SN, James TD, Crowell MD. 2000. Application of digital photogrammetry to complex topography for geomorphological research. *Photogrammetric Record* **16**: 793–821.

Lane SN, Reid SC, Westaway RM, Hicks DM. 2005. Remotely sensed topographic data for river channel research: the identification, explanation and management of error. In Spatial Modelling of the Terrestrial Environment. John Wiley & Sons: Chichester; 113–136.

Lane SN, Westaway RM, Murray HD. 2003. Estimation of erosion and deposition volumes in a large, gravel-bed, braided river using synoptic remote sensing. *Earth Surface Processes and Landforms* **28**: 249–271.

Laronne JB, Carson MA. 1976. Interrelationships between bed morphology and bed-material transport for a small, gravel-bed channel. *Sedimentology* **23**: 67–85.

Mankoff KD, Russo TA. 2013. The Kinect: a low-cost, high-resolution, short-range 3D camera. *Earth Surface Processes and Landforms* **38**: 926–936.

Mao L, Cooper JR, Frostick LE. 2011. Grain size and topographical differences between static and mobile armour layers. *Earth Surface Processes and Landforms* **36**: 1321–1334.

Millane RP, Weir MI, Smart GM. 2006. Automated analysis of imbrication and flow direction in alluvial sediments using laser-scan data. *Journal of Sedimentary Research* **76**: 1049–1055.

Nelson PA, Dietrich WE, Venditti JG. 2010. Bed topography and the development of forced bed surface patches. *Journal of Geophysical Research, Earth Surface* **115**: F04024.

Nikora VI, Goring DG, Biggs BJF. 1998. On gravel-bed roughness characterization. *Water Resources Research* **34**: 517–527.

Nitsche M, Turowski JM, Badoux A, Rickenmann D, Kohoutek TK, Pauli M, Kirchner JW. 2013. Range imaging: a new method for high-resolution topographic measurements in small- and medium-scale field sites. *Earth Surface Processes and Landforms* **38**: 810–825.

Ouédraogo MM, Degré A, Debouche C, Lisein J. 2014. The evaluation of unmanned aerial system-based photogrammetry and terrestrial laser scanning to generate DEMs of agricultural watersheds. *Geomorphology* **214**: 339–355.

Qin J, Zhong D, Wang G, Ng SL. 2012. On characterization of the imbrication of armored gravel surfaces. *Geomorphology* **159–160**: 116–124.

Rice SP, Church M. 2010. Grain-size sorting within river bars in relation to downstream fining along a wandering channel. *Sedimentology* **57**: 232–251.

Rice SP, Johnson MF, Reid I. 2012. Animals and the geomorphology of gravel-bed rivers. In Gravel-bed Rivers. John Wiley & Sons: Chichester; 225–241.

Rieke-Zapp DH, Rosenbauer R, Schlunegger F. 2009. A photogrammetric surveying method for field applications. *Photogrammetric Record* **24**: 5–22.

Robert A. 1991. Fractal properties of simulated bed profiles in coarse-grained channels. *Mathematical Geology* **23**: 367–382.

Rüther N, Huber S, Spiller S, Aberle J. 2013. Verifying a photogrammetric method to quantify grain size distribution of developed armor layers. *Proceedings of the 35th IAHR Congress*, Chengdu, China; 7.

Smart G, Aberle J, Duncan M, Walsh J. 2004. Measurement and analysis of alluvial bed roughness. *Journal of Hydraulic Research* **42**: 227–237.

Smith M, Vericat D, Gibbins C. 2012. Through-water terrestrial laser scanning of gravel beds at the patch scale. *Earth Surface Processes and Landforms* **37**: 411–421.

Smith MW, Vericat D. 2014. Evaluating shallow-water bathymetry from through-water terrestrial laser scanning under a range of hydraulic and physical water quality conditions. *River Research and Applications* **30**(7): 905–924.

Stumpf A, Malet JP, Allemand P, Pierrot-Deseilligny M, Skupinski G. 2015. Ground-based multi-view photogrammetry for the monitoring of landslide deformation and erosion. *Geomorphology* **231**: 130–145.

Verdú JM, Batalla RJ, Martínez-Casasnovas JA. 2005. High-resolution grain-size characterisation of gravel bars using imagery analysis and geo-statistics. *Geomorphology* **72**: 73–93.

Wackrow R, Chandler JH. 2008. A convergent image configuration for DEM extraction that minimises the systematic effects caused by an inaccurate lens model. *Photogrammetric Record* **23**: 6–18.

Wackrow R, Chandler JH, Bryan P. 2007. Geometric consistency and stability of consumer-grade digital cameras for accurate spatial measurement. *Photogrammetric Record* **22**: 121–134.